Energy Alignment and Recombination in Perovskite Solar Cells: Weighted Influence on the Open Circuit Voltage

Ilario Gelmetti[a,b‡], Núria F. Montcada[a‡], Ana Pérez-Rodríguez[c], Esther Barrena*[c], Carmen Ocal[c], Inés García-Benito[d], Agustín Molina-Ontoria[d], Nazario Martín[d,e]*, Anton Vidal-Ferran[a,f]* and Emilio Palomares[a,f]*

[a.] *Institute of Chemical Research of Catalonia (ICIQ). The Barcelona Institute of Science and Technology. Avda. Països Catalans, 16. Tarragona. E-43007. Spain.*
[b.] *Departament d'Enginyeria Electrònica, Elèctrica i Automàtica, Universitat Rovira i Virgili, Avda. Països Catalans 26, 43007 Tarragona, Spain*
[c.] *Institut de Ciència de Materials de Barcelona (ICMAB-CSIC), Campus UAB, Bellaterra 08193-Barcelona, Spain.*
[d.] *IMDEA-Nanociencia, C/ Faraday, 9, Campus de Cantoblanco, E-28049, Madrid, Spain.*
[e.] *Departamento de Química Orgánica I, Facultad de Ciencias Químicas, Universidad Complutense de Madrid, Madrid, Spain.*
[f.] *ICREA. Passeig Lluis Companys, 23. Barcelona. E-08010. Spain.*
**Author information: EP epalomares@icig.es*
‡ *These authors contributed equally to this work*

Abstract

In this work, we assess the possible reasons for the differences observed in open circuit voltage (V_{OC}) in mixed cation perovskite solar cells when comparing four different hole transport materials (HTMs), namely TAE-1, TAE-3, TAE-4 and spiro-OMeTAD. All these HTMs present close chemical and physical properties, however, once they are finally deposited onto the perovskite layer, the HTMs provide different performance characteristics. Additionally to the evaluation of the HTM influence on recombination, we find that, upon deposition of the organic HTM on top of the perovskite, there is an important change in the energy levels position, and the impact on the device V_{OC} is discussed. We consider that this experimental observation could be general for other organic HTMs and would justify the difficulties for finding molecules and materials that could improve the efficiency of perovskite solar cells overcoming the solar-to-energy conversion efficiency of solar cells made using spiro-OMeTAD as holes selective contact.

Introduction

Organic-inorganic lead halide perovskites have become the focus of intense research due to their outstanding performance in hybrid photovoltaic devices.[1] Perovskite solar cells without the use of HTM achieved efficiencies of 16 %,[2] way below the efficiencies of standard perovskite solar cells using HTMs.[1] Spiro-OMeTAD is the material of choice for most reported examples of triple cation (formamidinium, methylammonium, cesium) mixed halide (bromide, iodide) lead perovskite solar cells[3] with the FTO/d-TiO_2/CsFAMAPbIBr/HTM/Au structure, where FTO is fluorine doped tin oxide, d-TiO_2 is a dense layer of titania, and Au is the gold anode. In spite of the tremendous interest in developing novel HTMs for replacing the expensive spiro-OMeTAD, improving power conversion efficiency and cell stability, it is still unclear how to rationalize the HTM design. Although one significant design parameter for maximizing the V_{OC} is the position of the Highest Occupied Molecular Orbital (HOMO) level, a clear correlation is not always found among the published results.[4–9] A complication in determining the role of the HTM on device performance is that changing the HTM often affects other photophysical properties of the solar cell with significant impact on photovoltaic behaviour.

In a previous communication, aiming to match or improve the performance of the spiro-OMeTAD based devices, we reported the easy synthesis of a new organic HTM: TAE-1 (Figure 1).[10,11] However, despite its promising properties, with a slightly deeper oxidation potential in comparison with spiro-OMeTAD (Figure 2), the solar cells fabricated with TAE-1 were unable to overcome the V_{OC} values of the perovskite solar cell obtained using spiro-OMeTAD (Table 1).

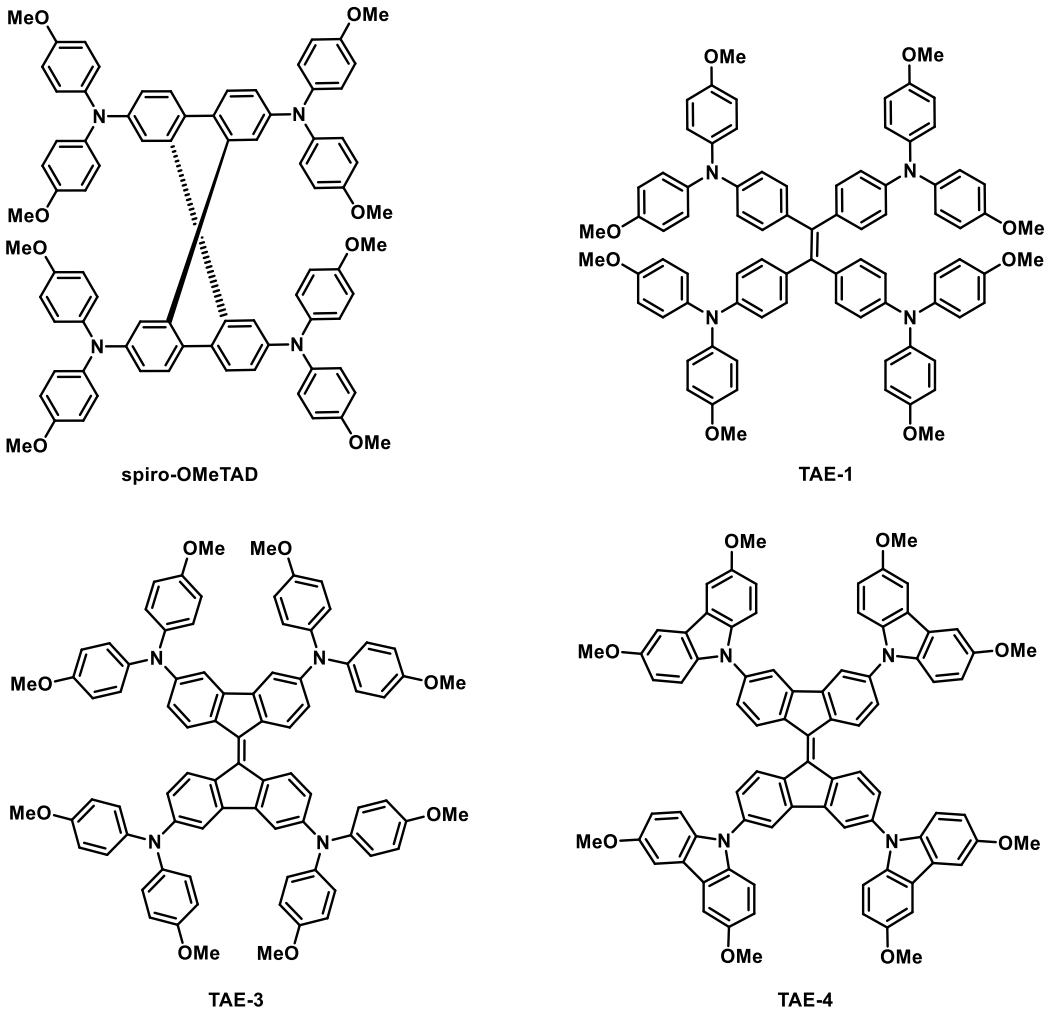

Figure 1. Molecular structures of spiro-OMeTAD, TAE-1, TAE-3 and TAE-4.

In this work, not only we replicate our observation on more HTMs, namely TAE-3 (3,3',6,6'-Tetrakis [N, N-bis(4-methoxyphenyl) amino]-9,9'-bifluorenylidene) and TAE-4 (3,3',6,6'-Tetrakis(3,6-dimethoxy-9H-carbazol-9-yl)-9,9'-bifluorenylidene, see Figure 1), but we also move one step further and get insight into the origin of the observed differences in V_{OC}. Unlike our previous communication,[10] where a 400 nm layer of mesoporous titanium oxide layer (m-TiO_2) was used as scaffold for the perovskite, herein we investigate the V_{OC} differences in planar junctions fabricated without this m-TiO_2 and depositing the perovskite layer directly over the dense titanium oxide layer (d-TiO_2) being the n-type selective contact. This architecture reduces the device complexity as one of the interfaces is supressed, the interfacial area between the ETL and perovskite is quite more defined, and ensures a complete coverage of the titanium oxide by the perovskite layer avoiding possible contacts between ETL and HTL that could create non-desired charge transfer pathways.

We evaluate in this study the influence of the molecular energetics, in other words, the different driving forces for the charge transfer process between the HTM and the perovskite (Figure 2), and the charge recombination between electrons at the perovskite and holes at the HTM on the V_{OC} observed in devices employing TAEs or spiro-OMeTAD. As the stack underlying the HTM is identical for all the studied devices, the relation between the V_{OC} and the electron transport material (ETM) or the perovskite characteristics[12] will not be considered.

The usage of advanced time-resolved techniques, such as Photo-Induced Charge Extraction (CE) and Photo-Induced Transient Photo-Voltage (TPV),[4,13] allows us to determine the impact of the HTM on the energetics distribution and charge recombination kinetics under different light intensities working conditions.[14–17] Further insight on the role of the interface energetics is provided by analysing the work function (WF), determined from contact potential difference (CPD) measured by Kelvin probe force microscopy (KPFM) in order to contrast the results obtained by CE and validate that method.[18,19]

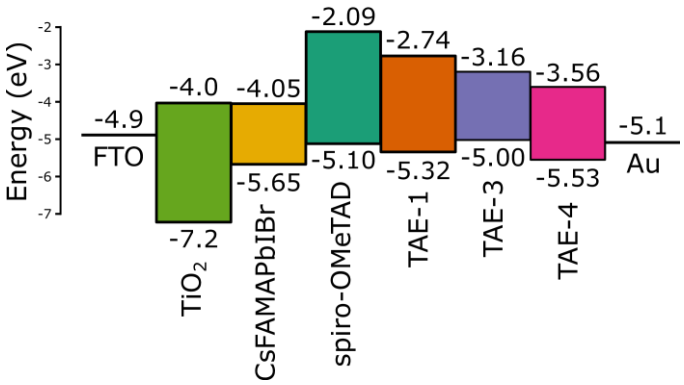

Figure 2. Schematics of the energy diagram for the materials in the perovskite solar cells studied in this work. The oxidation potential values approximating the HOMO of TAE-1, TAE-3, TAE-4 and spiro-OMeTAD have been extracted from cyclic voltammetry in solution (see Figure S11). The direct optical band gap has been determined by Tauc plot in solution (see Figures S19-S20).

Results and discussion

In a previous communication[10] we compared the novel TAE-1 molecule with the reference spiro-OMeTAD as HTM for methylammonium lead iodide perovskite solar cells with mesoporous TiO_2 as ETM. Here we investigate, in depth, the influence of the HTM on the V_{OC} of a triple cation perovskite solar cell with planar TiO_2 as ETM and we introduce two novel HTMs from the same family of TAE-1, which are TAE-3 and TAE-4.

These new derivatives were prepared following a straightforward two-step synthetic procedure. The synthetic route illustrated in Scheme S1 (see Supplementary Information for more details) allowed us to obtain TAE-3 and TAE-4. Firstly, 3,3',6,6'-Tetrabromo-9,9'-bifluorenylidene was obtained from a one-pot reaction by treating 3,6-dibromo-9H-fluoren-9-one, synthesised by

reported procedures,[10,20] in the presence of Lawesson's reagent in refluxing toluene. Finally, *p*-methoxydiphenylamine or 3,6- dimethoxy-9H-carbazole were covalently linked to the central unit by a four-fold Buchwald-Hartwig cross-coupling reaction to obtain TAE-3 and TAE-4 respectively in good yields. Complete structural characterization of the final compound TAE-3 and TAE-4 and the corresponding intermediates was accomplished using standard spectroscopic techniques such as ^{1}H NMR, ^{13}C NMR, FTIR, and UV-Visible (See Supporting Information). The ^{1}H NMR spectra of the final molecules reveal the characteristic signals of the bifluorenylidene core (two doublets and one double doublet corresponding to 4 protons each) and the representative signals of the donor units. In addition, mass spectrometry HRMS [MALDI-TOF] (Figure S3, S8) confirmed the presence of TAE-3 with a molecular ion peak $[M]^{+}$ at 1236.5029 $m{\cdot}z^{-1}$ and TAE-4 at 1228.4446 $m{\cdot}z^{-1}$. The hole mobility of the novel HTMs are not dissimilar to the spiro-OMeTAD one, being $5.9{\cdot}10^{-5}$, $8{\cdot}10^{-4}$, $7{\cdot}10^{-4}$ and $2.6{\cdot}10^{-4}$ $cm^{2}{\cdot}V^{-1}{\cdot}s^{-1}$ for TAE-1,[10] TAE-3, TAE-4 and spiro-OMeTAD[10] respectively (see Figure S12). Additionally to the experimental measurement of the oxidation potential of TAE-3 and TAE-4 (see Figure 2 and Figure S11), theoretical calculations have been used for predicting the HOMO and LUMO energies of all the novel HTMs (see Table S1 and Figures S13-S15). The oxidation potential of the HTMs follows the relation TAE-3 < spiro-OMeTAD < TAE-1 < TAE-4, being the HOMO of TAE-4 the closest to the valence band (VB) of the perovskite. We note that the values of HOMO derived from cyclic voltammetry oxidation potential, using a reported linear relation,[21] can differ from those obtained in the solid state for example by measuring ultraviolet photoelectron spectroscopy. Nonetheless, as a first approximation, we use these values with the complementarity of DFT theoretical results. Figure 2 illustrates the trend for the HOMO values as a result of our experimental and theoretical approach.[21] However, it is possible to have both a shift in the HOMO and LUMO energy or a change in the oxidative doping density upon deposition of the HTMs onto the perovskite thin film, as will be explained further in this paper.

The perovskite solar cells using as HTM either one of the TAEs or spiro-OMeTAD were fabricated using the procedure described in detail in the Supporting Information. All comparisons were carried out within the same set of solar cells and confirmed on at least two independent sets of devices. Every HTM was deposited by spin-coating obtaining similar thicknesses of ~50 nm (see Figure S29). The average and champion devices performance parameters are listed in Table 1; and Figure 3 shows the reverse current-voltage scans. The complete statistics, including forward scans data, scans at different velocities and at different illumination intensities, can be found in Figures S30-S39. The most interesting observation extracted from Table 1, and focused on the subject matter, is the larger V_{OC} in devices with spiro-OMeTAD, which is contrary to the

predicted dependence[22–24] of the V_{OC} with the ionization potential, i.e., a larger V_{OC} would be expected for TAE-1 and TAE-4 than for spiro-OMeTAD. The average V_{OC} of spiro-OMeTAD devices differs from those of TAE-1 and TAE-4 devices by 90 and 170 mV, respectively.

Table 1. Reverse scan solar cell parameters (short circuit current, open circuit voltage, fill factor, power conversion efficiency) for spiro-OMeTAD and TAEs devices.

Device	J_{SC} (mA·cm^{-2})	V_{OC} (V)	FF	PCE (%)
spiro-OMeTAD	23.0 (21.4±1.6)*	1.13 (1.07±0.06)	0.75 (0.68±0.11)	18.4 (15.6±3.1)
TAE-1	20.2 (20.2±0.9)	1.02 (0.98±0.03)	0.69 (0.60±0.10)	14.3 (11.8±2.1)
TAE-3	22.5 (22.5±1.9)	0.93 (0.89±0.04)	0.74 (0.71±0.06)	15.3 (14.1±1.4)
TAE-4	24.2 (21.0±1.8)	0.97 (0.90±0.06)	0.71 (0.61±0.09)	16.5 (11.6±2.8)

* The value in parenthesis are the average and standard deviation of 85 diodes for spiro-OMeTAD, 23 diodes for TAE-1, 29 diodes for TAE-3 and 21 diodes for TAE-4 (see Figure S30).

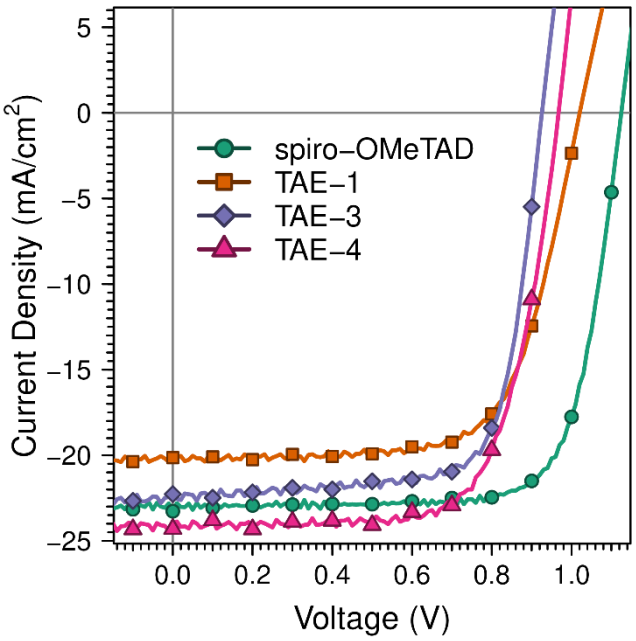

Figure 3. The current-voltage curves of the most representative perovskite devices using spiro-OMeTAD (green round points), TAE-1 (orange square points), TAE-3 (purple diamond points) and TAE-4 (magenta triangle points) as HTM under 1 sun conditions (1000 W·m^{-2}) and in reverse scan (forward curves are shown in Figure S31).

Performing the current-voltage scans at various light intensities, we obtained an ideality factor (see Figures S36-S39) of 1.57 for spiro-OMeTAD, 1.44 for TAE-1, 1.79 for TAE-3 and 1.83 for TAE-4, respectively. From this, we can state that the TAE-3 and TAE-4 trap states contributing to interfacial Shockley Read Hall (SRH) recombination are deeper in energy than those in spiro-OMeTAD and TAE-1.[25] We carried out time-resolved electrical measurements to assess how the HTM influences the free charges' distribution and recombination lifetime in the complete

devices. These time-resolved techniques allowed us, historically, to determine the different origin of recombination in other type of solar cells such as organic solar cells[17,26] and dye sensitized solar cells.[27,28] On the one hand, CE has been used previously to obtain the free carrier density in a device at different light bias (device V_{OC} at different light intensities), the charge distribution versus voltage, which is known to be very sensitive to the presence of additives[29–31], and differences in the HOMO energy level[32,33], leading to sensible shifts on the measured charge distribution. Charge extraction of devices has been measured using the same system as described in deep elsewhere by our group.[34] Due to the short measurement time window (10 µs, see Figure S40) we are not observing any contribution from ionic migration,[35] that would give a small and long lasting displacement current in larger time scales.[34,36] The charge distribution of all devices is obtained as shown in Figure 4 and each experimental curve can be fitted to a linear plus exponential dependence law. The linear component is caused by the geometric capacitance of free charges accumulating in the selective contacts.[13,17] Since this capacitance follows the parallel-plate capacitor model ($C=\varepsilon A/d$), with the main parameters being the thickness of the perovskite layer (d), its static permittivity (ε) and the active area of the device (A) no significant difference in thickness was observed for the different devices (see linear region in Figure 4), considering that the active area and the materials (perovskite and organic layer) are alike. Once the photo-induced quasi-Fermi splitting in the perovskite layer approaches the built-in potential (HTM HOMO and ETM LUMO energies difference) the depletion layers in the contacts start to saturate[19,37] and the photo-generated charges will be stored in the perovskite layer[38] increasing their chemical potential. This regime is commonly known as chemical capacitance or quantum capacitance and is revealed by an exponential increase in the charge versus light bias voltage plot. As can be observed in Figure 4 the voltage at which the chemical capacitance becomes relevant for each cell follows the trend TAE-4 < TAE-3 < TAE-1 < spiro-OMeTAD. From such shifts, we can infer that there is a difference in the in energy offsets respect to perovskite valence band (VB), with the most favourable alignment for spiro-OMeTAD. This is in correlation with the built-in voltage, and, as the ETM is the same for all the samples, also with the HTM HOMO energies, being spiro-OMeTAD the deepest. Interestingly, this order does not relate to the HOMO level as measured by solution cyclic voltammetry and shown in Figure 2. This can arise from differences between solution and solid state,[18,39–41] due to a chemical reactivity[42] or intermixing with the perovskite layer components.[19,43]

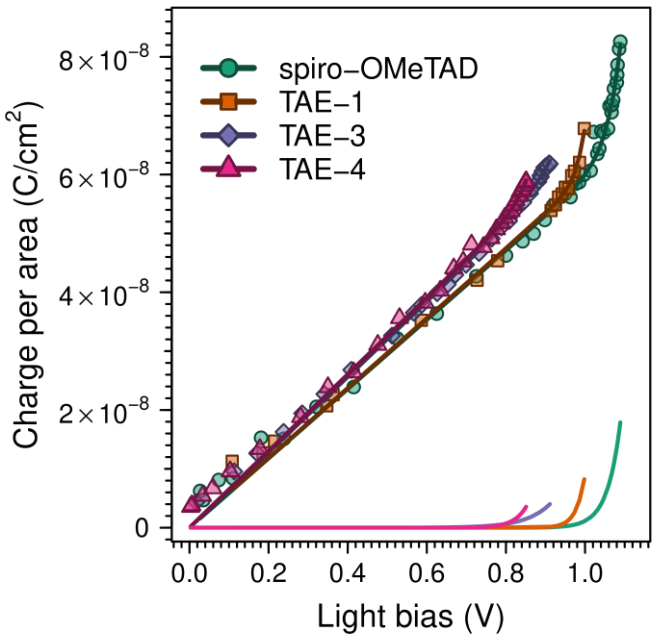

Figure 4. Charge from CE at different light bias voltages for solar cells with TAE-1, TAE-3,TAE-4 and spiro-OMeTAD. The dark solid lines are the data fits using a linear plus exponential model $y=Ax+Be^{Cx}$. The light colour solid lines at the graph bottom represent only the exponential part of the fits: $y=Be^{Cx}$.

When considering different HTMs for fabricating a perovskite solar cell, the resulting V_{OC} will mainly relate to the respective HOMO energy level,[44,45] as well as on the recombination constant[16] and density of states disorder.[46] In our case, we will not consider the density of states disorder as we presume that it will not differ significantly for molecules with such similar chemical structures as the ones studied here. Considering the HOMO energy, a deeper level, which is a bigger built-in voltage, allows the solar cell to reach a higher V_{OC}.[44,45,47] This intuitive relation can be rationalized as follows, considering the ETM/perovskite/HTM interfacial recombination:[25,48,49] (a) the V_{OC} is the applied voltage where the amount of recombination equals the amount of photo-generation; (b) the interfacial SRH recombination is proportional to the electrons or holes concentration in the perovskite at the interface with the HTM or ETM respectively;[50] (c) these concentrations increase after the filling of the contacts' depletion layers, which happens when the quasi-Fermi levels splitting in the perovskite (that is the origin of the V_{OC}[48,49]) approaches the built-in potential. Coherently, the aforementioned order of HOMO energies as obtained by the exponential onset in charge extraction (Figure 4) is reflected by the order of average V_{OC}s in Table 1: spiro-OMeTAD > TAE-1 > TAE-4 ≈ TAE-3.

In order to analyse first the influence of the recombination, we carried out TPV measurements on the devices under open circuit conditions. For all HTMs, the device's TPV transient decays (see Figure 5 and S41, S42) lead, through exponential decay fitting, to lifetimes at 1-sun illumination of the same order of magnitude, from 0.4 to 1.1 µs (see for each device the

rightmost point in Figure 5 and Figure S41). We can safely state that the bulk radiative recombination is negligible compared to the interfacial recombination as in cesium containing triple cation mixed halide perovskite the charges' diffusion length has been reported in the micrometre when isolated,[51] and gets notably reduced when sandwiched between an HTM and ETM extracting layers.[4] From the observation of the cross-sectional SEM (Figure S29) and top-view AFM (Figure S21, S24, S25, S26) and ESEM (Figure S22), we can also exclude the significant presence of pinholes in the perovskite layer. More interestingly, referring the transient decay lifetimes at different light intensities from TPV (see Figure S42) to the obtained chemical charge, subtracting the charge accumulated in the geometric capacitance, from CE (see Figure 4) we obtain a direct relationship between free charges lifetime and charge density in the perovskite layer, as shown in Figure 5. The choice of subtracting the charges accumulated in the contacts comes from the consideration that the interfacial SRH recombination is mainly influenced by changes in the low concentration of carriers in the perovskite layer rather than by the high concentration of majority carriers in the doped contacts.[34,50]

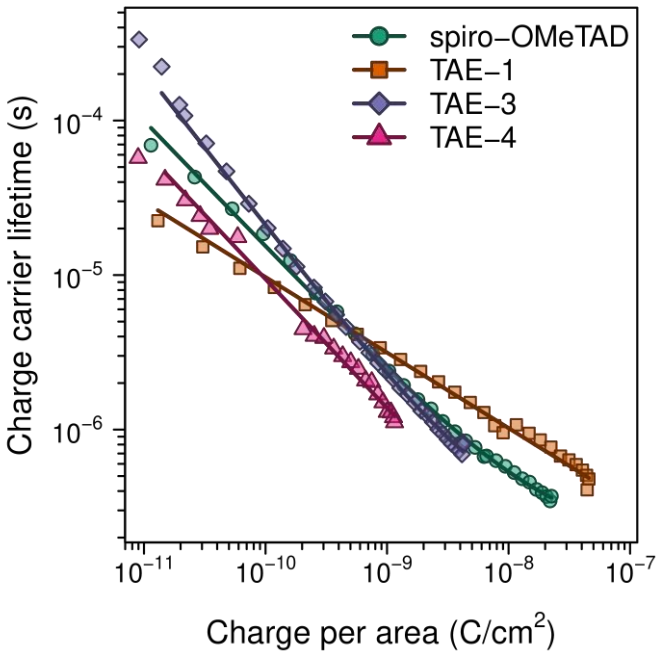

Figure 5. Charge carriers lifetime (obtained via TPV) at different chemical charge (as opposed to charges assigned to geometric capacitance, obtained from the exponential part of CE in Figure 4) of spiro-OMeTAD, TAE-1, TAE-3 and TAE-4 devices. The solid lines correspond to the respective fittings to a power law equation ($y=y_0+Ax^{-\lambda}$).[32]

As can be seen in Figure 5, the slopes for the all the devices are similar, indicating a common main carrier recombination pathway. In fact, the recombination order Φ obtained from the exponent λ of the power law fit (see caption of Figure 5, $\Phi = 1+\lambda$) is 1.5 for TAE-1 cell, 2.0 for TAE-3 cell, 1.8 for TAE-4 cell, and 1.8 for spiro-OMeTAD cell (values compatible with reports on surface recombination via deep-traps) indicating that the recombination between electrons

from the perovskite and holes from the HTM is the key loss mechanism in these devices and other recombination processes (at the contacts or due the transport of the charges) can be neglected.[25,52]

Further inspection of Figure 5 shows that the recombination lifetime at the same chemical charge density, for example at 10^{-9} C·cm^{-2}, though shorter for TAE-4 and longer for the other HTMs, does not drastically differ. However, the perceived tendency does not correspond to the trend observed in V_{OC} (Table 1).

Once demonstrated that the carrier recombination between the electrons in the perovskite and the holes in the distinct HTMs is not the key factor that determines the experimental V_{OC}, we examine next the impact in the vacuum level misalignment at the different heterojunctions.

To evaluate any possible deviation in the relative alignment of the HTMs´ HOMO on the FTO/d-TiO_2/CsFAMAPbIBr layer, as is suspected from CE results, the WF has been experimentally determined for the different layer stacks from CPD measurements via KPFM (see Supporting Information). As can be seen in Figure 6, the obtained WF of the FTO/d-TiO_2/CsFAMAPbIBr surface is 4.24±0.04 eV, which is comparable with the reported value for $MAPbI_3$ perovskite on *n*-type substrates.[55,56] When the HTMs are deposited on top of the perovskite, vacuum level (V_L) alignment is basically fulfilled for spiro-OMeTAD, TAE-1 and TAE-4, while the relative work function of TAE-3 with respect to that of the perovskite leads to an upward shift of the V_L as large as ~200 mV. This implies an upward shift of the HOMO of TAE-3 from the VB of the perovskite, within the band model.

It has been demonstrated that noticeable alterations in the electronic distribution can occur contacting the molecules designed as HTM with the perovskite layer induced by the generation of interfacial dipoles, enhancing or disfavouring the electric field that facilitates the charge separation and the extraction. This conformed a new parameter to take into account in the design of new molecules as hole transport materials in perovskite solar cells, which is not as easy to predict.

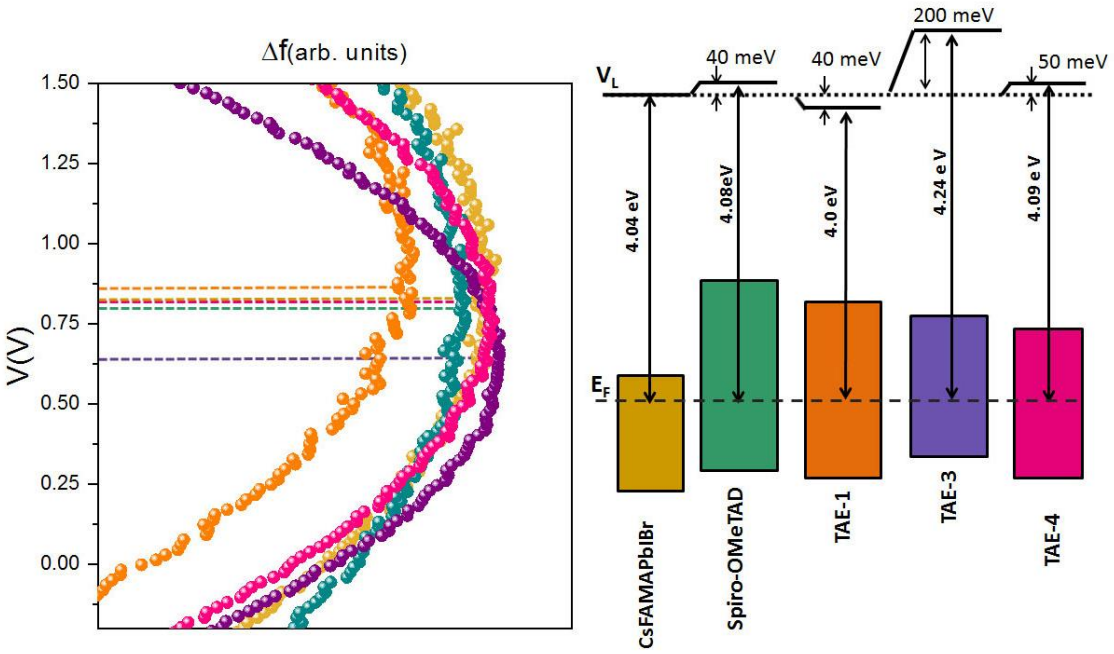

Figure 6. (left) CPD measurements between the KPFM tip and the surfaces of pristine CsFAMAPbIBr and the different HTMs devices (spiro-OMeTAD, TAE-1, TAE-3 and TAE-4). The corresponding WF values obtained from the parabolic fit of the data (see Supporting Information) are given in the schematics (right) of the proposed energy diagram. The corresponding vacuum level (V_L) shifts are obtained from the WF values.

In agreement with previous works[6,9] our results show that the design of new HTMs, for optimizing the solar cell performance and obtaining higher V_{OC} in the heterojunction, does not only consist of lowering the HOMO energy level. Notwithstanding that the lower V_{OC} for TAE-3 can be correlated with its less favourable energy alignment with the perovskite and its larger interfacial recombination with respect to the other HTMs, the fact is that for TAE-1, TAE-4 and spiro-OMeTAD the V_{OC} shows no correlation with the corresponding HOMO level position.

The whole experimental data and analysis presented here suggest that for the design of novel HTMs that aim to overcome the solar to energy conversion of the spiro-OMeTAD careful analysis of the energetics at the interface between the organic semiconductor material and the perovskite must be taken into account in conjunction with carrier mobility properties and interfacial carrier recombination processes.

Conclusions

We present a thorough investigation with the aim of shedding light on the underlying reason for the changes of the open-circuit voltage in mixed cation perovskite solar cells using two already known and two unpublished hole transporting materials: spiro-OMeTAD, TAE-1, TAE-3 and TAE-4, all with quite similar chemical structure. The choice of these HTMs is not arbitrary as they contain the most common moieties used in the myriad of novel HTMs described in the scientific

literature focussed on perovskite solar cells. We observe how the energy levels as obtained by cyclic voltammograms are a valid starting point when trying to predict the device characteristics. However, as we have demonstrated, it is possible that the HOMO energy values differ importantly when the organic semiconductor molecule is deposited on top of the perovskite semiconductor material.

By means of photo-induced charge extraction we have been able to obtain a better indication of the HOMO level position of the HTM when layered in a solar cell stack. Kelvin probe force microscopy has been employed as local probe for confirming the work function actually in place in a complete and functional device. Complementing this experimental information with the study of the interfacial recombination processes in solar cell operando conditions -via photo-induced transient photovoltage - has allowed us to disentangle the complex influence of the HTM on the device photovoltaic performances. The shift of the energy levels of the TAEs molecules upon contact with the perovskite layer is, together with changes in recombination rate, influencing the measured V_{OC} values which are notably different from the expected ones attending to the HOMO energy values inferred from cyclic voltammetry experiments further supported by advanced DFT calculations.

We have shown that the design of HTM to reach the expected maximum theoretical efficiency in perovskite solar cells will require fine tuning of the energetics at the interface between the HTM and the perovskite, for instance the use of self assembled monolayer of molecular dipoles, etc…, without increase the interfacial carrier recombination processes between the HTM and the semiconductor perovskite.

References

1 M. A. Green, Y. Hishikawa, E. D. Dunlop, D. H. Levi, J. Hohl-Ebinger and A. W. Y. Ho-Baillie, *Prog. Photovoltaics Res. Appl.*, 2018, **26**, 427–436.

2 Y. Li, S. Ye, W. Sun, W. Yan, Y. Li, Z. Bian, Z. Liu, S. Wang and C. Huang, *J. Mater. Chem. A*, 2015, **3**, 18389–18394.

3 M. Saliba, T. Matsui, J.-Y. Seo, K. Domanski, J.-P. Correa-Baena, M. K. Nazeeruddin, S. M. Zakeeruddin, W. Tress, A. Abate, A. Hagfeldt and M. Grätzel, *Energy Environ. Sci.*, 2016, **9**, 1989–1997.

4 J. Jiménez-López, W. Cambarau, L. Cabau and E. Palomares, *Sci. Rep.*, 2017, **7**,

6101.

5 A. Abate, M. Planells, D. J. Hollman, V. Barthi, S. Chand, H. J. Snaith and N. Robertson, *Phys. Chem. Chem. Phys.*, 2015, **17**, 2335–2338.

6 L. E. Polander, P. Pahner, M. Schwarze, M. Saalfrank, C. Koerner and K. Leo, *APL Mater.*, 2014, **2**, 081503.

7 S. M. Park, S. M. Mazza, Z. Liang, A. Abtahi, A. M. Boehm, S. R. Parkin, J. E. Anthony and K. R. Graham, *ACS Appl. Mater. Interfaces*, 2018, **10**, 15548–15557.

8 N. Ishida, A. Wakamiya and A. Saeki, *ACS Photonics*, 2016, **3**, 1678–1688.

9 R. A. Belisle, P. Jain, R. Prasanna, T. Leijtens and M. D. McGehee, *ACS Energy Lett.*, 2016, **1**, 556–560.

10 L. Cabau, I. Garcia-Benito, A. Molina-Ontoria, N. F. Montcada, N. Martin, A. Vidal-Ferran and E. Palomares, *Chem. Commun.*, 2015, **51**, 13980–13982.

11 H. Choi, K. Do, S. Park, J.-S. Yu and J. Ko, *Chem. - A Eur. J.*, 2015, **21**, 15919–15923.

12 C. Bi, Q. Wang, Y. Shao, Y. Yuan, Z. Xiao and J. Huang, *Nat. Commun.*, 2015, **6**, 7747.

13 I. Gelmetti, L. Cabau, N. F. Montcada and E. Palomares, *ACS Appl. Mater. Interfaces*, 2017, **9**, 21599–21605.

14 T. Du, J. Kim, J. Ngiam, S. Xu, P. R. F. Barnes, J. R. Durrant and M. A. McLachlan, *Adv. Funct. Mater.*, 2018, **28**, 1801808.

15 J. M. Marin-Beloqui, J. P. Hernández and E. Palomares, *Chem. Commun.*, 2014, **50**, 14566–14569.

16 J. M. Marin-Beloqui, L. Lanzetta and E. Palomares, *Chem. Mater.*, 2016, **28**, 207–213.

17 J. W. Ryan and E. Palomares, *Adv. Energy Mater.*, 2017, **7**, 1601509.

18 A. Opitz, *J. Phys. Condens. Matter*, 2017, **29**, 133001.

19 I. M. Hermes, Y. Hou, V. W. Bergmann, C. J. Brabec and S. A. L. Weber, *J. Phys.*

Chem. Lett., 2018, 6249–6256.

20 B. Wang, Z. Xie, Y. Li, Z. Yang and L. Chen, *Macromolecules*, 2018, **51**, 3443–3449.

21 B. W. D'Andrade, S. Datta, S. R. Forrest, P. Djurovich, E. Polikarpov and M. E. Thompson, *Org. Electron. physics, Mater. Appl.*, 2005, **6**, 11–20.

22 H.-Y. Chen, J. Hou, S. Zhang, Y. Liang, G. Yang, Y. Yang, L. Yu, Y. Wu and G. Li, *Nat. Photonics*, 2009, **3**, 649–653.

23 Y. S. Kwon, J. Lim, H.-J. Yun, Y.-H. Kim and T. Park, *Energy Environ. Sci.*, 2014, **7**, 1454.

24 K. Rakstys, A. Abate, M. I. Dar, P. Gao, V. Jankauskas, G. Jacopin, E. Kamarauskas, S. Kazim, S. Ahmad, M. Grätzel and M. K. Nazeeruddin, *J. Am. Chem. Soc.*, 2015, **137**, 16172–16178.

25 P. Calado, D. Burkitt, J. Yao, J. Troughton, T. M. Watson, M. J. Carnie, A. M. Telford, B. C. O'Regan, J. Nelson and P. R. F. Barnes, 2018, arXiv:1804.09049.

26 D. Fernandez, A. Viterisi, V. Challuri, J. W. Ryan, E. Martinez-Ferrero, F. Gispert-Guirado, M. Martinez, E. Escudero, C. Stenta, L. F. Marsal and E. Palomares, *ChemSusChem*, 2017, **10**, 3118–3134.

27 M. Godfroy, C. Aumaitre, F. Caffy, Y. Kervella, L. Cabau, L. Pellejà, P. Maldivi, S. Narbey, F. Oswald, E. Palomares, D. Joly and R. Demadrille, *Dye. Pigment.*, 2017, **146**, 352–360.

28 P. R. F. Barnes, K. Miettunen, X. Li, A. Y. Anderson, T. Bessho, M. Grätzel and B. C. O'Regan, *Adv. Mater.*, 2013, **25**, 1881–1922.

29 B. C. O'Regan, K. Bakker, J. Kroeze, H. Smit, P. Sommeling and J. R. Durrant, *J. Phys. Chem. B*, 2006, **110**, 17155–17160.

30 S. Nakade, T. Kanzaki, W. Kubo, T. Kitamura, Y. Wada and S. Yanagida, *J. Phys. Chem. B*, 2005, **109**, 3480–3487.

31 Y.-C. Chang, H.-P. Wu, N. M. Reddy, H.-W. Lee, H.-P. Lu, C.-Y. Yeh and E. W.-G. Diau, *Phys. Chem. Chem. Phys.*, 2013, **15**, 4651.

32 D. Credgington, R. Hamilton, P. Atienzar, J. Nelson and J. R. Durrant, *Adv. Funct. Mater.*, 2011, **21**, 2744–2753.

33 A. Sánchez-Díaz, M. Izquierdo, S. Filippone, N. Martin and E. Palomares, *Adv. Funct. Mater.*, 2010, **20**, 2695–2700.

34 B. C. O'Regan, P. R. F. Barnes, X. Li, C. Law, E. Palomares and J. M. Marin-Beloqui, *J. Am. Chem. Soc.*, 2015, **137**, 5087–5099.

35 C. Eames, J. M. Frost, P. R. F. Barnes, B. C. O'Regan, A. Walsh and M. S. Islam, *Nat. Commun.*, 2015, **6**, 7497.

36 D. Moia, I. Gelmetti, P. Calado, W. Fisher, M. Stringer, O. Game, Y. Hu, P. Docampo, D. Lidzey, E. Palomares, J. Nelson and P. R. F. Barnes, 2018, arXiv:1805.06446.

37 F. Fabregat-Santiago, G. Garcia-Belmonte, I. Mora-Seró and J. Bisquert, *Phys. Chem. Chem. Phys.*, 2011, **13**, 9083.

38 V. W. Bergmann, Y. Guo, H. Tanaka, I. M. Hermes, D. Li, A. Klasen, S. A. Bretschneider, E. Nakamura, R. Berger and S. A. L. Weber, *ACS Appl. Mater. Interfaces*, 2016, **8**, 19402–19409.

39 P. Sehati, S. Braun and M. Fahlman, *Chem. Phys. Lett.*, 2013, **583**, 38–41.

40 F. Bussolotti, J. Yang, A. Hinderhofer, Y. Huang, W. Chen, S. Kera, A. T. S. Wee and N. Ueno, *Phys. Rev. B*, 2014, **89**, 115319.

41 T. Breuer, A. Karthäuser and G. Witte, *Adv. Mater. Interfaces*, 2016, **3**, 1500452.

42 J. Carrillo, A. Guerrero, S. Rahimnejad, O. Almora, I. Zarazua, E. Mas-Marza, J. Bisquert and G. Garcia-Belmonte, *Adv. Energy Mater.*, 2016, **6**, 1502246.

43 S. Kim, S. Bae, S.-W. Lee, K. Cho, K. D. Lee, H. Kim, S. Park, G. Kwon, S.-W. Ahn, H.-M. Lee, Y. Kang, H.-S. Lee and D. Kim, *Sci. Rep.*, 2017, **7**, 1200.

44 C. J. Brabec, A. Cravino, D. Meissner, N. S. Sariciftci, T. Fromherz, M. T. Rispens, L. Sanchez and J. C. Hummelen, *Adv. Funct. Mater.*, 2001, **11**, 374–380.

45 A. Gadisa, M. Svensson, M. R. Andersson and O. Inganäs, *Appl. Phys. Lett.*, 2004, **84**, 1609–1611.

46 N. K. Elumalai and A. Uddin, *Energy Environ. Sci.*, 2016, **9**, 391–410.

47 C. Uhrich, D. Wynands, S. Olthof, M. K. Riede, K. Leo, S. Sonntag, B. Maennig and

M. Pfeiffer, *J. Appl. Phys.*, 2008, **104**, 043107.

48 M. Stolterfoht, P. Caprioglio, C. M. Wolff, J. A. Márquez, J. Nordmann, S. Zhang, D. Rothhart, U. Hörmann, A. Redinger, L. Kegelmann, S. Albrecht, T. Kirchartz, M. Saliba, T. Unold and D. Neher, 2018, arXiv:1810.01333.

49 M. Stolterfoht, C. M. Wolff, J. A. Márquez, S. Zhang, C. J. Hages, D. Rothhardt, S. Albrecht, P. L. Burn, P. Meredith, T. Unold and D. Neher, *Nat. Energy*, 2018, **3**, 847–854.

50 W. Shockley and W. T. Read, *Phys. Rev.*, 1952, **87**, 835–842.

51 S. Liu, W. Huang, P. Liao, N. Pootrakulchote, H. Li, J. Lu, J. Li, F. Huang, X. Shai, X. Zhao, Y. Shen, Y.-B. Cheng and M. Wang, *J. Mater. Chem. A*, 2017, **5**, 22952–22958.

52 A. Baumann, K. Tvingstedt, M. C. Heiber, S. Väth, C. Momblona, H. J. Bolink and V. Dyakonov, *APL Mater.*, 2014, **2**, 081501.

53 T. Kirchartz, B. E. Pieters, J. Kirkpatrick, U. Rau and J. Nelson, *Phys. Rev. B*, 2011, **83**, 115209.

54 Y.-C. Shih, L. Wang, H.-C. Hsieh and K.-F. Lin, *ACS Appl. Mater. Interfaces*, 2018, **10**, 11722–11731.

55 E. M. Miller, Y. Zhao, C. C. Mercado, S. K. Saha, J. M. Luther, K. Zhu, V. Stevanović, C. L. Perkins and J. van de Lagemaat, *Phys. Chem. Chem. Phys.*, 2014, **16**, 22122–22130.

56 S. Olthof and K. Meerholz, *Sci. Rep.*, 2017, **7**, 40267.

Acknowledgements

EP and AVF thank MINECO (projects CTQ2013-47183 and CTQ2014-60256-P). NM thanks European Research Council (ERC-320441-Chirallcarbon), the CAM (FOTOCARBON project S2013/MIT-2841) and the Spanish Ministry of Economy and Competitiveness MINECO (projects CTQ2014-52045-R and CTQ2015-71154-P). NM also thanks Alexander von Humboldt Foundation. EP and AV are also grateful to ICIQ and ICREA for economical support. EB and CO thank MAT2016-77852-C2-1-R (AEI/FEDER, UE) the Generalitat de Catalunya 2014 SGR501 and

also they acknowledge the MINEICO project MAT2015-68994-REDC. IG thanks Jesús Jiménez-López for the fruitful discussions.

Author contributions

NFM and IG contributed equally to this work. IG prepared the solar cells. IG and NFM measured current-voltage curves. IG carried out the CE and TPV experiments. NFM measured mobility via SCLC. EP and NFM designed the experiments and supervised the experimental part. EP, NFM and IG interpreted the data measured using CE and TPV. AV carried out the HOMO-LUMO calculations and UVvis simulations. NM and AM designed the TAE-1, TAE-3 and TAE-4. IGB synthesized the molecules. APR, EB and CO performed and analysed the Kelvin probe force microscopy contact potential measurements. The manuscript was written through contributions of all authors. All authors have given approval to the final version of the manuscript.

Additional Information

Supplementary information accompanies this paper.

Competing Interests: The authors declare no competing financial interests.